Journal of Magnetism and Magnetic Materials 391 (2015) 108–115

Contents lists available at ScienceDirect

Journal of Magnetism and Magnetic Materials

journal homepage: www.elsevier.com/locate/jmmm

Cr-substituted Ni–Zn ferrites via oxalate decomposition. Structural, electrical and magnetic properties

M.A. Gabal [a,*,1], Y.M. Al Angari [a], F.A. Al-Agel [b]

[a] Chemistry department, Faculty of Science, King Abdulaziz University, Jeddah, KSA
[b] Physics department, Faculty of Science, King Abdulaziz University, Jeddah, KSA

ARTICLE INFO

Article history:
Received 22 February 2015
Received in revised form
23 April 2015
Accepted 24 April 2015
Available online 29 April 2015

Keywords:
Cr-substitution
NiZn ferrite
Susceptibility
Hysteresis
Conductivity

ABSTRACT

A series of Cr-substituted Ni–Zn ferrites; $Ni_{0.8}Zn_{0.2}Cr_xFe_{2-x}O_4$ (x=0.0–1.0) were prepared via oxalate decomposition route to characterize the effect of Cr-substitution on structural, magnetic and electrical properties. The prepared powders were characterized using X-ray diffraction (XRD), Fourier transform infrared (FT-IR) and transmission electron microscopy (TEM). XRD indicated single-phase cubic ferrites. The lattice parameters (a_{Exp}) exhibited a gradual decrease with increasing chromium, attributed to the smaller ionic radii of Cr^{3+} substituent. According to the obtained structural data, an appropriate cation distribution was suggested and fortified through FT-IR spectroscopy besides magnetic and electrical measurements. TEM image showed agglomerated cubic crystals with an average size of about 20 nm. Vibrating sample magnetometer (VSM) measurements indicated minimal hysteresis characteristic for soft magnetic material. The decrease in saturation magnetization (M_s) with Cr-substitution was discussed in view of Neel's two sub-lattice model. The change in the coercivity with Cr-content was discussed in view of estimated cation distribution and magnetization values. The obvious fall in the Curie temperature, estimated from molar susceptibility measurements, with increasing Cr-concentrations was assigned to the gradual replacement of Fe^{3+} ions on the octahedral sites by paramagnetic Cr^{3+} ions. ac-conductivity as a function of both frequency and absolute temperature exhibited a semi-conducting behavior. The decrease in conductivity with increasing Cr-content was attributed to the preferential occupation of Cr^{3+} ions by octahedral sites which replacing Fe^{3+} ions and limiting Fe^{2+}–Fe^{3+} conduction.

© 2015 Elsevier B.V. All rights reserved.

1. Introduction

Ni–Zn ferrites are soft ferrimagnetic ceramic materials with superior many technological applications due to their high permeability at high frequency, remarkably high-electrical resistivity, low-eddy current loss, and reasonable cost [1,2]. They are commonly used in high frequency transformer cores and inductors, microwave devices, radars, antenna rods, high-speed digital tape or disk recording, etc. [3].

Ni–Zn ferrite is a well-known mixed inverse spinel with unit cell consisting of eight formula units of the form: $(Zn_xFe_{1-x})[Ni_{1-x}Fe_{1+x}]O_4$ [4]. The intrinsic magnetization of the system is thus depending on the inverse and normal phase, i.e., the distribution of cations in the spinel lattice. The cationic substitution induces changes in the structure and texture of the crystal, resulting in significant modifications in the magnetic and electrical properties [5]. The understanding of these changes provides information on which the reliable formulation of ferrites suitable for specific applications can be based.

Few researchers have been reported on the effect of paramagnetic substitution with Cr^{3+} ions on the electromagnetic properties of Ni–Zn ferrites. El-Sayed [6] studied the effect of Cr-substitution in NiZn ferrite on the structure, density, porosity, shrinkage and grain size. The results showed a decreasing trend with increasing Cr-content.

El-Sayed [5] also explained the electrical conductivity of these ferrites in terms of their cation distribution and revealed the predominance of the hopping conduction mechanism.

Costa et al. [3] studied the effect of Cr^{3+} on the morphological and magnetic properties of Ni–Zn ferrites produced by the combustion reaction. The obtained ferrites, with an average crystallite sizes between 21 and 26 nm, exhibited saturation magnetizations in the range of 43–53 emu/g, which showed a gradual decrease with increasing Cr.

Birajdar et al. [7] prepared Cr-substituted Ni–Zn ferrites with

---

[*] Corresponding author.
E-mail address: mgabalabdonada@yahoo.com (M.A. Gabal).
[1] Permanent address: Chemistry Department, Faculty of Science, Benha University, Benha, Egypt.

http://dx.doi.org/10.1016/j.jmmm.2015.04.115
0304-8853/© 2015 Elsevier B.V. All rights reserved.

the formula $Ni_{0.7}Zn_{0.3}Cr_xFe_{2-x}O_4$ ($x=0.0$–0.5) via sol–gel auto-combustion method. The results showed that the bulk density and crystallite size decrease with increasing chromium content whereas porosity and coercivity increase.

The processing methods are known also to affect the different properties of ferrites as they can result in different cation distributions or sizes. Many methods were developed for preparing ferrites [8–11]. To the best of our knowledge, there is no reported results on the preparation of Cr-substituted Ni–Zn ferrites through the thermal decomposition reaction of their respective oxalates.

Devising methods to organize functional magnetic nanostructures for the quest of magnetic materials leads to the production of different properties [12]. In the present study, we will report on the preparation of $Ni_{0.8}Zn_{0.2}Cr_xFe_{2-x}O_4$ ferrites ($x=0.0$–1.0) via oxalate decomposition process. The decomposition route and ferrites formation will be followed using differential thermal analysis-thermogravimetry techniques (DTA-TG). The prepared ferrites will be characterized using X-ray diffraction (XRD), Fourier transform infrared spectroscopy (FT-IR) and transmission electron microscopy (TEM) measurements. The magnetic properties will be measured through vibrating sample magnetometer (VSM) and DC-magnetic susceptibility (as a function of magnetic field strength and temperature) measurements. In addition, the electrical properties as a function of frequency and temperature will be also measured. The effect of Cr-substitution and the entire processing method on the structural, magnetic and electrical properties of Ni–Zn ferrites will be estimated and discussed.

2. Experimental procedures

Cr-substituted Ni–Zn nano-crystalline ferrites with a general formula $Ni_{0.8}Zn_{0.2}Cr_xFe_{2-x}O_4$ ferrites ($x=0.0$–1.0) were synthesized by impregnation technique [13–15]. All chemicals were analytical grade and used without any further purification. In a typical experiment, the nickel nitrate $Ni(NO_3)_2\cdot 6H_2O$, zinc nitrate $Zn(NO_3)_2\cdot 6H_2O$, ferric nitrate $Fe(NO_3)_3\cdot 9H_2O$, chromium oxide; Cr_2O_3 and oxalic acid; $H_2C_2O_4\cdot 2H_2O$ were used as starting materials. The respective metal oxalates were prepared through precipitation method in which oxalic acid solution was added under vigorous stirring to metal nitrate solution and the obtained precipitate was collected by filtration followed by drying in oven at 100 °C.

For the preparation of the precursors, stoichiometric ratios of metal oxalates were mixed thoroughly in a mortar using water drops to ensure homogeneity. The obtained dry precursors were calcined in an electric furnace at 1000 °C for 2 h and the obtained powders were stored in a desiccator.

Thermogravimetric (TG) and differential thermal analysis (DTA) of the dried precursor was carried out using Perkin Elmer STA 6000 thermal analyzer up to 1000 °C at a heating rate of 5 °C min^{-1} in air atmosphere.

Structural characterization was carried out on a Bruker D8 Advance X-ray diffractometer with Cu-Kα radiation (step time 8 s; step size 0.02 °; $2\theta=10$–70 °). The average particle size was calculated using the most intense peak (311) applying the Scherrer formula [14].

FT-IR spectra in the range 300–700 cm^{-1} were recorded using a JASCO FT-IR 310 spectrometer. The powders were mixed with spectral grade KBr as the standard.

TEM studies were carried out using Jeol (JEM-1011 electron microscopy) operated at 100 kV.

Magnetic measurements were performed using the vibrating sample magnetometer (VSM; 9600-1 LDJ, USA) with a maximum applied field of 5 kOe at room temperature.

Dc-magnetic susceptibility were measured using Faraday's method [14]. The measurements were performed as a function of temperature from room temperature up to 800 K and different magnetic field intensities (660, 1010, 1340 and 1660 Oe).

The electrical measurements, viz. ac-conductivity and dielectric measurements were carried out on a Hioki LCR high tester 3531 (Japan) using the two-probe method. The samples in a powdered form were compressed to pellets of 1 cm diameter and about 1 mm thickness using a pressure of 2 t cm^{-2}. The two surfaces were polished and coated with silver paint. The temperature was raised up to 823 K and the frequency was changed in the range (100 Hz–5 MHz).

3. Results and discussion

3.1. Thermal decomposition process and ferrite formation

The thermal decomposition behavior of the oxalate precursor in air, with $x=0.2$ as a representative study, was followed up to ferrite formation. Fig. 1 exhibits the simultaneous DTA-TG curves up to 1000 °C. From the figure, it is clear that the weight loss starts at 123 °C with the release of 1.5% up to 140 °C attributed to the loss of 0.4 water molecules (experimentally calculated = 1.4%). The second weight loss step sets on 165 °C with a steep slope up to 207 °C, exhibiting a weight loss of 17.2% agreed well with the theoretically calculated loss due to the release of remaining water molecules from the precursor. Two endothermic DTA peaks with peaks temperatures at 133 and 189 °C are characterizing these two dehydration steps.

The decomposition process of the formed anhydrous precursor is followed immediately after the dehydration process showing three well-defined TG steps up to 385 °C. These steps are attributed, according to the obtained weight losses and decomposition ranges to the decomposition of ferrous, nickel and zinc oxalates content, respectively [13]. The weight loss of the first step up to about 280 °C amounts to 20.5% agreed well with the theoretically calculated of 20.4% attributed to the decomposition of ferrous oxalate content into iron(III) oxide. The very sharp exothermic DTA peak at 232 °C characterizes well this oxidative decomposition process.

The nickel oxalate content of the precursor decomposed exothermically in the following step showing 11.6% weight loss assigned to the formation of NiO (calculated weight loss = 11.5%). The accompanying exothermic DTA peak at 332 °C is attributed to the oxidation of nickel metal decomposition product [16].

In the last weight loss step, amounts to 2.9%, the zinc oxalate content decomposed to ZnO with the release of CO and CO_2. The closely corresponding exothermic DTA peak at 347 °C is due to the oxidation of CO byproduct to CO_2 [16].

After the complete decomposition of the oxalates content the

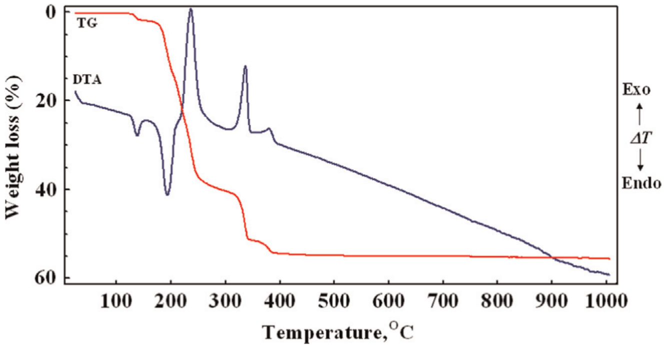

Fig. 1. DTA-TG curves in air of precursor with Cr-content of 0.2. Heating rate = 5 °C min^{-1}.

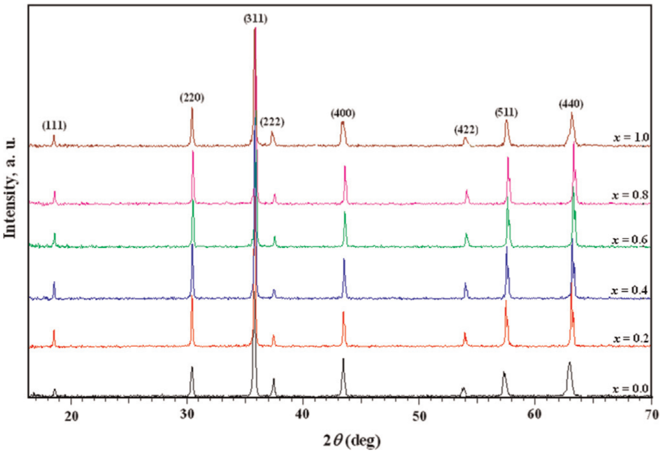

Fig. 2. XRD patterns of the $Ni_{0.8}Zn_{0.2}Cr_xFe_{2-x}O_4$ system.

final decomposition product is expected to contain mixed oxides of Fe_2O_3, NiO, ZnO and Cr_2O_3 and no further weight loss was observed above 385 °C. The very broad endothermic DTA peak appeared in the range 870–1000 °C without any accompanying weight loss can be assigned to the ferrite formation reaction [13]. This result suggests that the appropriate calcination temperature for ferrites formation for the precursors under investigation is about 1000 °C.

3.2. structural characterization

3.2.1. X-ray diffraction

X-ray measurements were performed to identify the single-phase structure of the investigated samples. Fig. 2 shows the structural characterization for the entire precursors calcined at 1000 °C carried out by XRD technique. All the samples showed single-phase cubic spinel structure without any indication for the presence of any intermediate phases. The values of the experimental lattice parameters (a_{Exp}) as a function of chromium content are calculated using Bragg's equation [14] and are reported in Table 1. It can be seen that the lattice parameters decreases proportionally with increasing Cr-content. This decrease can be explained, based on the Vegard’s law [17], to the difference in ionic radii of Fe^{3+} (0.645 Å) and Cr^{3+} ions (0.615 Å) [18]. A similar behavior was reported for other Cr-substituted ferrites [11,14,19–21].

The X-ray densities (D_x) were calculated using the molecular weights and lattice constants of the entire ferrites using relation from [14]. The reported values in Table 1 showed a very slight change with increasing substitution. This normal behavior since, the decrease in the weight with Cr-substitution is accompanied by a decrease in the lattice parameters.

The average crystallite sizes (L) were calculated using the line broadening and applying the Scherrer's equation [21]. The given data in Table 1 exhibited very slight decrease in sizes with increasing substitution.

In the present ferrite system; $Ni_{0.8}Zn_{0.2}Cr_xFe_{2-x}O_4$ it is well known that Ni^{2+} and Cr^{3+} ions have a great preference for the octahedral (B) sites [14,22] whereas, Zn^{2+} ion have strong preference for the tetrahedral (A) sites [13,22] while Fe^{3+} ions can exist at both sites though they prefer the B site [22]. According to these preferences, the suggested cation distribution formula of the present system can be written as

$$(Zn_{0.2}Fe_{0.8})^A[Ni_{0.8}Fe_{1.2-x}Cr_x]^BO_4$$

This distribution indicates that the Cr^{3+} ions only substitute the Fe^{3+} ions present in the B-sites while ions located in the A-sites remained unchanged. An exception was obtained with Cr-content (x = 1.0), in which chromium is observed to be partially distributed between the two sites. This behavior will be discussed using FT-IR spectroscopy measurements.

The theoretical lattice parameters (a_{th}) calculated (Table 1) according to the above proposed cation distribution using equation from [14] showed, a close agreement with those experimentally estimated suggesting the suitability of the proposed cation distribution in representing the system.

The cation radii (r_A and r_B), oxygen positional parameters (u), hopping lengths (L_A and L_B) in both tetrahedral and octahedral sites, tetrahedral bond length d_{AO}, the octahedral bond length d_{BO}, tetrahedral edge d_{AE} octahedral edge d_{BE} and unshared edge d_{BEU} as well as the inversion factor (γ) [i.e. amount of iron present in tetrahedral sites] were calculated using equations from [14] and reported in Table 1.

The values of cationic radii calculated based on the proposed cationic distribution indicated constant r_A with slightly decreasing r_B values by increasing chromium content. This explains why the lattice parameters decrease by substitution and suggests that the substitution strongly influenced octahedral B sites.

The values of oxygen positional parameters are observed to be slightly higher than the ideal values of 0.375 [22]. This value is well known to be dependent on the chemical composition, preparation conditions and heating procedure. The constant values obtained suggest that the chromium ions substitute only the iron present in the octahedral sites.

The hopping lengths (L_A, L_B) calculated are observed to decrease with increasing Cr content. This is can be explained based on the smaller ionic radii of Cr-substituent than that of iron which makes the ions close to each other and decreasing hopping length.

The interionic distances between the cations M–M and between cations and anion M–O are slightly decreased with increasing Cr-content. This result agrees well with the decrease in the lattice parameters [23].

3.2.2. FT-IR spectral study

FT-IR spectra of the entire Cr-substituted Ni–Zn ferrites, recorded at room temperature in the frequency range 700–300 cm^{-1}, are shown in Fig. 3. The bands positions at different Cr-content were summarized in Table 2. The higher frequency band; ν_1 (582–606 cm^{-1}) and the lower frequency band;

Table 1
Structural data of $Ni_{0.8}Zn_{0.2}Cr_xFe_{2-x}O_4$ system.

Cation distribution	a, (Å)		r, (Å)		L (nm)	D_X (g cm^{-3})	γ	u (Å)	L_A (Å)	L_B (Å)	d_{AO} (Å)	d_{BO} (Å)	d_{AE} (Å)	D_{BE} (Å)	D_{BEU} (Å)
	a_{exp}	a_{th}	r_A	r_B											
$(Zn_{0.2}Fe_{0.8})[Ni_{0.8}Fe_{1.2}]O_4$	8.3589	8.3609	0.512	0.663	96	5.36	0.8	0.381	3.619	2.959	1.897	2.041	3.097	2.813	2.957
$(Zn_{0.2}Fe_{0.8})[Ni_{0.8}Fe_{1.0}Cr_{0.2}]O_4$	8.3490	8.3529	0.512	0.660	107	5.36	0.8	0.381	3.615	2.956	1.894	2.038	3.094	2.810	2.954
$(Zn_{0.2}Fe_{0.8})[Ni_{0.8}Fe_{0.8}Cr_{0.4}]O_4$	8.3328	8.3449	0.512	0.657	95	5.38	0.8	0.381	3.608	2.950	1.891	2.034	3.088	2.805	2.948
$(Zn_{0.2}Fe_{0.8})[Ni_{0.8}Fe_{0.6}Cr_{0.6}]O_4$	8.3272	8.3369	0.512	0.654	91	5.37	0.8	0.381	3.606	2.948	1.889	2.033	3.085	2.803	2.946
$(Zn_{0.2}Fe_{0.8})[Ni_{0.8}Fe_{0.4}Cr_{0.8}]O_4$	8.3194	8.3289	0.512	0.651	91	5.37	0.8	0.381	3.602	2.945	1.888	2.031	3.083	2.800	2.943
$(Zn_{0.2}Fe_{0.6}Cr_{0.2})[Ni_{0.8}Fe_{0.4}Cr_{0.8}]O_4$	8.3188	8.3228	0.508	0.651	89	5.35	0.6	0.381	3.602	2.945	1.887	2.031	3.082	2.799	2.943

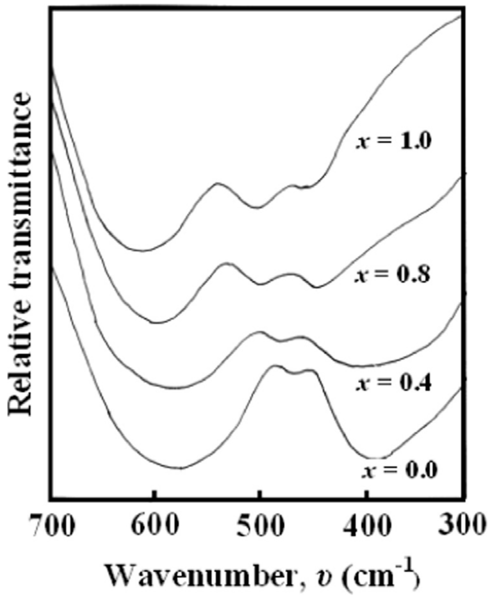

Fig. 3. FT-IR spectra of $Ni_{0.8}Zn_{0.2}Cr_xFe_{2-x}O_4$ system.

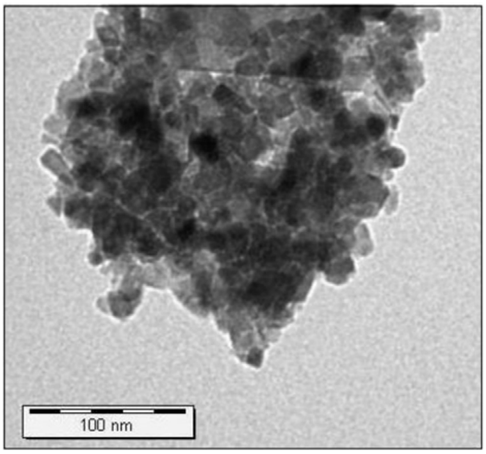

Fig. 4. TEM image of the sample with $x=0.0$.

ν_2 (400–454 cm^{-1}) are assigned, according to Waldron [24], to the stretching vibrations in the tetrahedral and octahedral sites, respectively. The higher vibration of the tetrahedral sites compared with that of octahedral sites can be due to the shorter bond length of the tetrahedral cluster and the longer bond length of the octahedral cluster.

The results showed very slight change in the bands positions up to $x=0.8$ with a sudden increase at $x=1.0$ for the tetrahedral sites, while that of the octahedral sites exhibited a gradual increase with increasing Cr-content. This gradual increase can be attributed, in accordance with the calculated ionic radii; r_B (Table 1), to the variation in the cation–oxygen bond length in the octahedral lattice of the spinel. The displacement of larger Fe^{3+} ions by smaller Cr^{3+} ions will result in decreasing the metal–oxygen bond length and consequently increasing frequency. The very slight change in the tetrahedral sites bands positions; ν_1 agreed well with the reported tetrahedral ionic radii; r_A (Table 1) indicating constant composition up to $x=0.8$. The sudden increase in the band position at $x=1.0$ suggests the preferential occupation of Cr^{3+} ions in this sites at these high concentrations. Similar behaviors are reported in literature for Cr-substituted $NiFe_2O_4$ [14,25].

The splitting of the ν_2 band may be attributed to increasing the quantity of Cr^{3+}–O^{2-} complexes as the Fe^{3+} content decreases at the B-sites. Similar splitting in the FT-IR spectra have been reported in literature for the Cr^{3+} substituted ferrite system [14,26,27].

The spectra also exhibited a decreasing trend in the intensity of the ν_2 band with increasing Cr-content, which can be due to the perturbation occurring in Fe–O bonds by Cr^{3+}-substitution. The intensity ratio is a function of the change of dipole moment with the internuclear distance ($d\mu/dr$) and the gradual substitution with Cr^{3+} ions, having $3d^4 4s^2$ orbitals, affecting the electronic distribution of Fe–O bonds and consequently the $d\mu/dr$ value [6].

3.2.3. TEM

Typical TEM image of the entire Cr^{3+} substituted Ni–Zn ferrites system ($x=0.0$) is shown in Fig. 4. The image shows agglomerated cubic crystals with an average size of about 20 nm, which is obviously smaller than that estimated through X-ray measurements. The agglomeration phenomenon occurred due to the tendency of the particles to reduce their surface area and achieving lower energy. In addition, the magneto-static interaction between particles or the experience of the nanoparticles for a permanent magnetic moment proportional to their volume cannot be neglected [28].

3.3. Magnetic properties

3.3.1. Hysteresis measurements

Fig. 5 shows the variation of magnetization as a function of Cr-content as well as magnetic field strength for the entire ferrite system. The hysteresis curves can help in understanding the magnetic behavior of the investigated samples besides providing information regarding some magnetic parameters such as saturation magnetization (M_s), magnetic moment (η_B), coercivity (H_c), remanent magnetization (M_r) and loop squareness ratio (M_r/M_s). The curves indicate the characteristics of soft magnetic material with minimal hysteresis. The different magnetic parameters were estimated and summarized in Table 2.

The variation of the saturation magnetization as well as the coercivity on the amount Cr substitution is illustrated in Fig. 6. From the figure, it is obvious that, the saturation magnetization

Table 2
FT-IR spectral data and electromagnetic parameters of $Ni_{0.8}Zn_{0.2}Cr_xFe_{2-x}O_4$ system.

x	ν_1 (cm^{-1})	ν_2 (cm^{-1})	Hysteresis loop					$\eta_B(x)$	Magnetic susceptibility		σ (ohm^{-1} cm^{-1})	ΔE_1 (eV)	ΔE_2 (eV)
			M_S	M_r	M_r/M_S	H_C	η_B		χ_M	T_C			
0.0	582	400	71.5	11.5	0.16	9.2	3.02	3.74	11.0	783	1.4×10^{-6}	0.22	0.31
0.2	582	421	46.8	7.5	0.16	12.4	1.97	3.34	11.8	718	3.1×10^{-7}	0.31	0.35
0.4	585	426	38.0	8.5	0.22	24.6	1.59	2.94	6.7	658	2.4×10^{-7}	0.32	0.48
0.6	582	444	29.2	7.8	0.27	25.1	1.22	2.54	5.6	605	1.5×10^{-7}	0.37	0.50
0.8	587	445	18.0	6.2	0.34	32.1	0.75	2.14	3.9	573	2.1×10^{-8}	0.50	0.52
1.0	605	454	10.3	4.1	0.40	48.6	0.43	2.54	2.5	548	1.1×10^{-7}	0.52	0.60

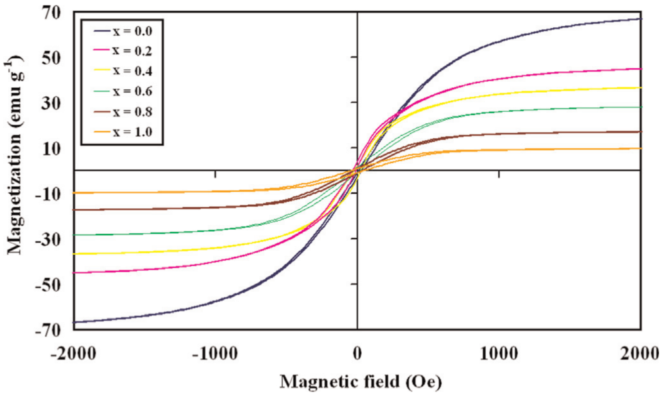

Fig. 5. Hysteresis loops for $Ni_{0.8}Zn_{0.2}Cr_xFe_{2-x}O_4$ system.

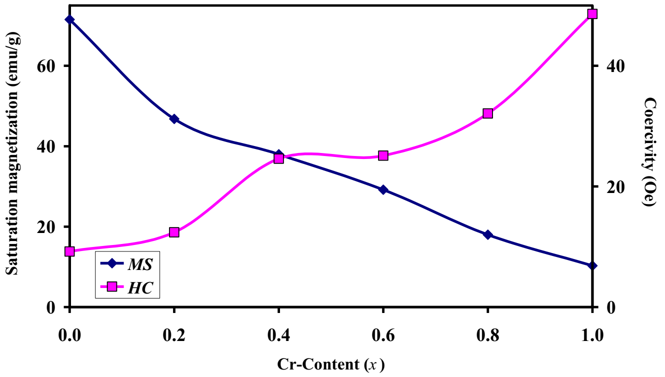

Fig. 6. Variation of the saturation magnetization and coercivity with x in $Ni_{0.8}Zn_{0.2}Cr_xFe_{2-x}O_4$ system.

decreases gradually with increasing Cr-substitution while coercivity increases. In addition, the remanent magnetization as well as the experimental magnetic moment (η_B) per formula unit in Bohr magneton [14], exhibits a decreasing trend with increasing substitution.

The saturation magnetization value obtained in the present work for $Ni_{0.8}Zn_{0.2}Fe_2O_4$ (i.e. the sample without Cr-substitution) is apparently higher than those reported in the literature [29–32] instead; the coercivity value is relatively lower. The decrease in the values of M_s and consequently the accompanying magnetic moment parameter with the addition of Cr^{3+} ions can be discussed in the view of Neel's two sub-lattice model of ferrimagnetism [33].

In ferrites, the magnetic moment due to the uncompensated electron spin and the spin alignments of the individual ions in the tetrahedral A-sites is found to be anti-parallel to those in the octahedral B-sites. According to Neel's model, the A–B super-exchange interactions predominate the A–A and B–B interactions. The net theoretical magnetic moment per formula unit was calculated, using the suggested cation distribution, from the equation: $\eta_B(x)=M_B(x) - M_A(x)$ where, M_A and M_B are the magnetic moments of A and B sublattices and the ionic magnetic moments of Fe^{3+}, Ni^{2+}, Cr^{3+} and Zn^{2+} are 5.0, 2.18, 3.0 and 0.0 BM, respectively [34].

The obtained results reported in Table 2 showed a decreasing trend as those determined by the hysteresis loop (η_B). The Cr^{3+} ions preferentially occupy octahedral B sites. Thus, the gradual replacement of highly magnetic Fe^{3+} located in the octahedral sites by lower magnetic Cr^{3+} ions reduces the magnetic moment as well as the exchange interactions of the sublattice [35].

The disagreement between the experimental (η_B) and calculated magnetic moment $\eta_B(x)$ values at different Cr-content (Table 2) suggested that, the Cr^{3+} moments (located at the B-sites) are aligned anti-parallel to the A-site moments and indicating non-collinear structure [36]. In addition, the effect of canted or triangular lattice arrangements of the magnetic moments cannot be neglected [23,37].

The cation distribution estimated using XRD and FT-IR measurements clearly indicated that Cr^{3+} ions occupying the octahedral sites up to $x=0.8$ however, for the composition $x>0.8$ they prefer tetrahedral sites. This behavior agrees well with the calculated Neel's magnetic moments (Table 2) where, the ferrite samples with $x<0.8$ have Nèel type magnetic order while for those with $x>0.8$ the Neel's theory do not remain valid. Similar results are reported in literature for Cr-substituted ferrites systems [14,25,38].

Fig. 6 obviously showed that the coercivity increases slowly up to $x=0.8$ after which it increases steeply. This behavior may be understood as mentioned by Banerjee and O'Reilly [39] on the basis of new cation distribution model. As already discussed in XRD and FT-IR results the chromium ions prefer to occupy the tetrahedral sites at these higher concentrations causing a negative trigonal field to be superimposed on the Cr^{3+} ions in the octahedral sites. Thus, a two-fold degeneracy of orbital ground state results in an unquenched orbital angular momentum and a large anisotropy [25].

The coercivity is known as an independent parameter, which can be altered by heat treatment or deformation. This increase in the coercivity by increasing Cr concentration can be related to the change in saturation magnetization through Brown's relation [40]:$H_c = \frac{2K_1}{\mu_0 M_s}$, in which the coercivity is inversely proportional to the saturation magnetization value, which agrees will with the present results.

The low values of the remanent magnetization M_r (Table 2) can be attributed to the low saturation magnetization as well as the nano-sized characteristics [23]. The lower values of the loop squareness ratio (M_r/M_s) obtained (less than 0.5) suggested that the particles could interact by magnetostatic interactions [41] and recommend the using of these materials for low inductance cores and coils [34].

3.3.2. Magnetic susceptibility measurements

Fig. 7 illustrates the change in the molar magnetic susceptibility (χ_M) as a function of both magnetic field strength and absolute temperature up to 800 K. The obvious decrease in the susceptibilities by increasing magnetic field intensity can be considered as a normal magnetic behavior attributed to the saturation of the magnetic domains [14]. The molar magnetic susceptibility (χ_M) measured at room temperature and 1010 G are summarized in Table 2 from which it is noticed that, χ_M decreases linearly with increasing Cr-content.

All the ferrite samples up to $x=0.6$ exhibits normal ferromagnetic behavior with χ_M decreases gradually by increasing temperature until reaching the Curie point (T_C) after which paramagnetic characters predominates. The samples with higher Cr-content showed a very week ferromagnetic behavior or nearly behave paramagnetically. The magnetic parameters were calculated from $1/\chi_M$ vs. T plot and the obtained values at different Cr-content, of Curie temperature (T_C) at field strength of 1010 G were reported in Table 2.

The Curie temperature for $Ni_{0.8}Zn_{0.2}Fe_2O_4$, prepared through flash combustion technique [42], was ≥ 485 °C. This relatively higher temperature was attributed to the lower Zn-content which increases the interaction between Ni^{2+} ions located in the octahedral sites and Fe^{3+} ions present in the tetrahedral sites. It is well known that [43], Curie temperature depends on the type of cations and their sites distribution, which in turn depends on the preparation method, calcination conditions and grain size. Thus, the

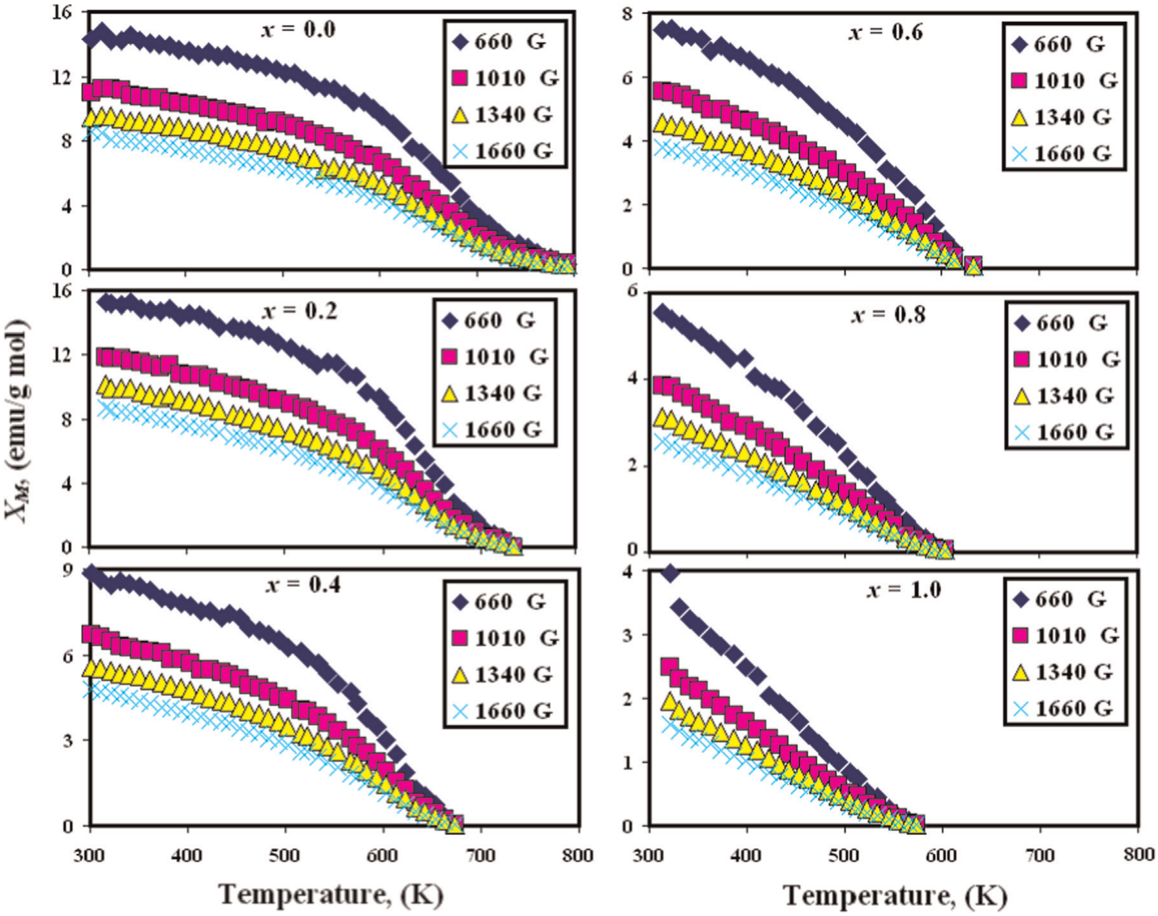

Fig. 7. Relation between molar magnetic susceptibility and absolute temperature as a function of different magnetic field intensities for $Ni_{0.8}Zn_{0.2}Cr_xFe_{2-x}O_4$ system.

slightly higher T_C obtained in the present study (Table 2) for pure Ni–Zn ferrite may be attributed to the preparation method as well as the obtained grain size.

The obvious fall in the Curie temperature with increasing Cr-concentrations (Table 2) can be assigned to the gradual replacement of Fe^{3+} ions on the octahedral sites by less magnetic or paramagnetic Cr^{3+} ions [44]. This substitution will decreases the B-sublattice magnetization without affecting the A-sublattice, which in turn weakens A–B exchange interaction and decreases Curie temperature.

3.4. Electrical conductivity measurements

Fig. 8 illustrates the ac-conductivity behaviors of the Cr-substituted $Ni_{0.8}Zn_{0.2}Fe_2O_4$ system as a function of both frequency and absolute temperature. The temperature dependence relations exhibit a semi-conducting behavior for all investigated samples in which conductivity increases with increasing temperature.

At low temperatures, the electrical conductivities obtained are observed to be frequency dependant while frequency independent at high temperatures. The pumping force of the frequency at low temperatures, facilate the transferring of the charge carriers besides liberating the trapped charges from the different trapping centers. On the other hand, at high temperatures, the large lattice vibration generated scatters the charge carriers and overcome the effect of frequency.

By increasing temperature, two well-defined regions are obtained which are characteristic for are the samples. In the first region, the thermal energy is not enough for librating charge carriers and conductivity hardly changed with temperature. In the second region, the conductivity increased linearly with temperature exhibiting a weak anomaly at the medium temperature region.

The room temperature conductivity values calculated at 100 kHz as a function of Cr-content are summarized in Table 2. The results showed a gradual decrease in the conductivity with increasing Cr-substitution. In cubic ferrites [21], the conduction is mainly due to the hopping between ions with mixed valence. In this context, the Verwey-de Boer mechanism suggested the hopping between statistically distributed Fe^{2+} and Fe^{3+} ions at the two equivalent crystallographic A and B-sites. The distance between the ions at octahedral B-sites is very small compared to that between ions at B-site and tetrahedral A-site. This will consequently increase the probability of B–B electron hopping compared to that of B–A. The A–A hopping does not exist, since only Fe^{3+} ions are exist at A-sites and all Fe^{2+} ions formed during the calcination process prefer to occupy B-sites [14]. Since, chromium ions have only one oxidation state thus they will not participate in the conduction process. Their preferential occupation by octahedral sites will replace Fe^{3+} ions and consequently results in limiting Fe^{2+}–Fe^{3+} conduction degree [45]. This will hinder the Verwey-de Boer mechanism and resulting in the conductivity decrease.

The very slight increase in the conductivity value observed for Cr-content; $x = 1.0$ can be attributed to the change in the preferential occupation of Cr^{3+} ions from octahedral to tetrahedral sites as appeared from the estimated cation distribution previously discussed.

The change in the slope of $\ln\sigma$ vs. $1000/T$ by increasing temperature indicated a change in the conduction mechanism. The

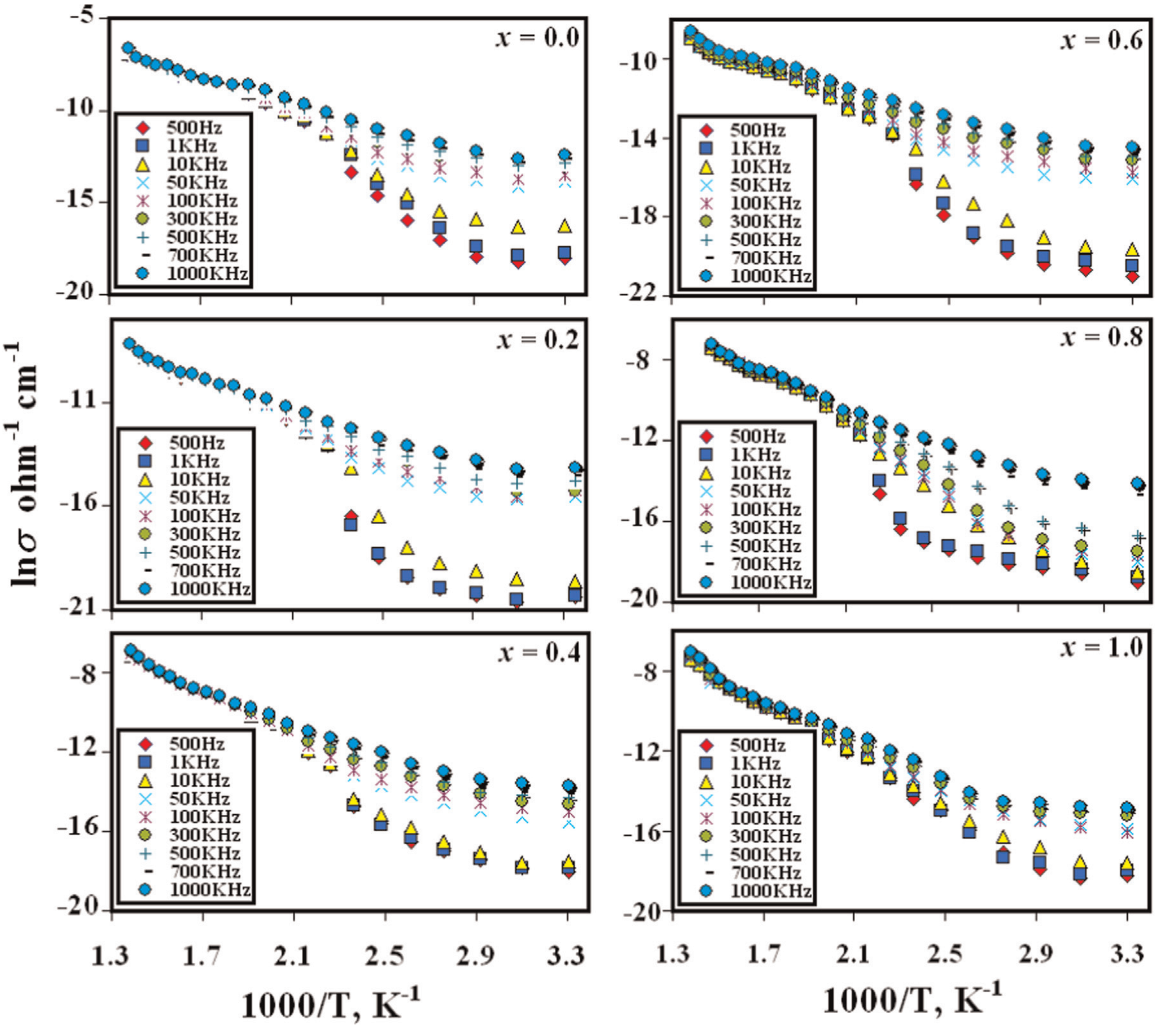

Fig. 8. Relation between lnσ and reciprocal of absolute temperature at different Cr-content as a function of applied frequency for $Ni_{0.8}Zn_{0.2}Cr_xFe_{2-x}O_4$ system.

linear fit to the Arrhenius relation: $\sigma = \sigma_0 e^{\frac{-\Delta E}{K_B T}}$ where K_B is the Boltzmann constant gives the hopping activation energy (ΔE) [46]. The variation of the activation energies ΔE_1 and ΔE_2 calculated at low and high temperature regions, respectively with chromium content (at frequency of 500 kHz) are represented in Table 2. The activation energies obtained were observed to increase with increasing Cr-content and the higher activation energy corresponds to the lower conductivity (Table 2).

The obtained activation energy at lower temperatures region (ΔE_1) is observed to be lower than that obtained at high temperatures region (ΔE_2). Generally, the conduction at lower temperature can be attributed to the electrons hopping between Fe^{2+} and Fe^{3+} ions, whereas that at higher temperature can be assigned to polaron hopping which need higher activation energy [47].

4. Conclusions

Cr-substituted Nickel–Zinc ferrites; $Ni_{0.8}Zn_{0.2}Cr_xFe_{2-x}O_4$ (x=0.0–1.0) were synthesized through oxalate decomposition reaction. XRD patterns revealed pure spinel cubic ferrites. The lattice parameters decrease with increasing Cr-content whereas; X-ray densities exhibited a very slight change with increasing substitution. The substitution obviously affects the magnetic and electrical properties of the system. The saturation magnetization was found to decrease with increasing Cr-content, whereas coercivity increases. The investigated samples showed a semiconducting behavior by increasing temperature and exhibited a decrease in conductivity with increasing Cr-content. The fall in the Curie temperature by Cr-substitution indicated the replacement of Fe^{3+} ions at octahedral sites by Cr^{3+} ions. An appropriate cation distribution was suggested and was fortified through structural, magnetic and electrical measurements.

Acknowledgment

This project was funded by the Deanship of Scientific Research (DSR), King Abdulaziz University, Jeddah, under grant No. [116/130/1434]. The authors, acknowledge with thanks DSR technical and financial support.

References

[1] A. Goldman, Modern Ferrite Technology, 2nd ed., Springer, New York, 2006.
[2] R.V. Mangalaraja, S. Ananthakumar, P. Manohar, F.D. Gnanam, Mater. Sci. Eng. A 355 (2003) 320–324.
[3] A.C.F.M. Costa, V.J. Silva, H.S. Ferreira, A.A. Costa, D.R. Cornejo, R.H.G. A. Kiminamid, L. Gama, J. Alloys Compd. 483 (2009) 655–657.
[4] R.C. O'Handley, Modern Magnetic Materials-Principles and Applications, Wiley-IEEE Press, New York, 2000.
[5] A.M. El-Sayed, Mater. Chem. Phys. 82 (2003) 583–587.
[6] A.M. El-Sayed, Ceram. Int. 28 (2002) 651–655.

[7] A.A. Birajdar, Sagar E. Shirsath, R.H. Kadam, S.M. Patange, K.S. Lohar, D. R. Mane, A.R. Shitre, J. Alloys Compd. 512 (2012) 316–322.
[8] I. Ali, M.U. Islam, M. Ishaque, H.M. Khan, M.N. Ashiq, M.U. Rana, J. Magn. Magn. Mater. 324 (2012) 3773–3777.
[9] S. Gubbala, H. Nathani, K. Koizol, R.D.K. Misra, Physica B 348 (2004) 317–328.
[10] J. Peng, M. Hojamberdiev, Y. Xu, B. Cao, J. Wang, H. Wu, J. Magn. Magn. Mater. 323 (2011) 133.
[11] M.A. Gabal, Mater. Lett. 64 (2010) 1887–1890.
[12] S.B. Darling, S.D. Bader, J. Mater. Chem. 15 (2005) 4189–4195.
[13] M.A. Gabal, Y.M. Al-Angari, Mater. Chem. Phys. 115 (2009) 578–584.
[14] M.A. Gabal, Y.M. Al Angari, Mater. Chem. Phys. 118 (2009) 153–160.
[15] M.A. Gabal, Y.M. Al Angari, M.W. Kadi, Polyhedron 30 (2011) 1185–1190.
[16] D. Dollimore, Thermochim. Acta 117 (1987) 331–363.
[17] C.G. Whinfrey, D.W. Eckort, A. Tauber, J. Am. Chem. Soc. 82 (1960) 2695–2697.
[18] R.D. Shannon, Acta Crystallogr. Sect. A 32 (1976) 751–767.
[19] M. Hashim, S. Alimuddin, S.E. Kumar, R.K. Shirsath, H. Kotnala, Chung, R. Kumar, Powder Technol. 229 (2012) 37–44.
[20] A.A. Birajdar, S.E. Shirsath, R.H. Kadam, S.M. Patange, K.S. Lohar, D.R. Mane, A. R. Shitre, J. Alloys Compd. 512 (2012) 316–322.
[21] S. Bhukal, T. Namgyal, S. Mor, S. Bansal, S. Singhal, J. Mol. Struct. 1012 (2012) 162–167.
[22] J. Smit, H.P.J. Wijn, Ferrites, Philips Technical Library, Eindhovan, 1959.
[23] A.I. Borhan, T. Slatineanu, A.R. Iordan, M.N. Palamaru, Polyhedron 56 (2013) 82–89.
[24] R.D. Waldron, Phys. Rev. 99 (1955) 1727–1735.
[25] S. Singhal, K. Chandra, J. Solid State Chem. 180 (2007) 296–300.
[26] S.M. Patange, Sagar E. Shirsath, B.G. Toksha, S.S. Jadhav, S.J. Shukla, K. M. Jadhav, Appl. Phys. A: Mater Sci. Process A95 (2009) 429–434.
[27] F.A. Lopez, A. Lopez-Delgado, J.L. Martın de Vidales, E. Vila, J. Alloys Compd. 265 (1998) 291–296.
[28] E. Manova, B. Kunev, D. Paneva, I. Mitov, L. Petrov, C. Estourne, s, C. D'Orle, J. L. Rehspringer, M. Kurmoo, Chem. Mater. 16 (2004) 5689–5696.
[29] T. Jahanbin, M. Hashim, K.A. Matori, S.B. Waje, J. Alloys Compd. 503 (2010) 111–117.
[30] T. Slatineanu, A.R. Iordan, M.N. Palamaru, O.Fl Caltun, V. Gafton, L. Leontie, Mater. Res. Bull. 46 (2011) 1455–1460.
[31] A.K.M. Akther Hossain, S.T. Mahmud, M. Seki, T. Kawai, H. Tabata, J. Magn. Magn. Mater. 312 (2007) 210–219.
[32] Z. Beji, L.S. Smiri, M.J. Vaulay, F. Herbst, S. Ammar, F. Fievet, Thin Solid Films 518 (2010) 2592–2598.
[33] L. Neel, C.R. Acad., Sci. Paris 230 (1950) 375.
[34] A.K. Ghatage, S.C. Choudhary, S.A.J. Patil, Mater. Sci. Lett. 15 (1996) 1548–1550.
[35] G.L. Sun, J.B. Li, J.J. Sun, X.Z. Yang, J. Magn. Magn. Mater. 281 (2004) 173–177.
[36] J.M. Hastings, L.M. Corliss, Phys. Rev. 126 (1962) 556–565.
[37] A. Pradeep, P. Priyadharsini, G. Chandrasekaran, J. Alloys Compd. 509 (2011) 3917–3923.
[38] A.K. Ghatage, S.A. Patil, S.K. Paranjpe, Solid State Commun. 98 (1996) 885–888.
[39] S.K. Banerjee, W. O'Reilly, IEEE Trans. Magnets 3 (1966) 463–467.
[40] J.M.D. Coey, Rare Earth Permanent Magnetism, John Wiley and Sons, New York, 1996.
[41] L. Gama, E.P. Hernandez, D.R. Cornejo, A.A. Costa, S.M. Rezende, R.H.G. A. Kimimami, A.C.F.M. Costa, J. Magn. Magn. Mater. 317 (2007) 29–33.
[42] R.V. Mangalaraja, S. Ananthakumar, P. Manohar, F.D. Gnanam, J. Magn. Magn. Mater. 253 (2002) 56–64.
[43] P. Gao, X. Hua, V. Degirmenci, D. Rooney, M. Khraisheh, R. Pollard, R. M. Bowman, E.V. Rebrov, J. Magn. Magn. Mater. 348 (2013) 44–50.
[44] A. Lakshman, K.H. Rao, R.G. Mendiratta, J. Magn. Magn. Mater. 250 (2002) 92–97.
[45] S.C. Watawe, B.D. Sarwade, S.S. Bellad, B.D. Sutar, B.K. Chougule, J. Magn. Magn. Mater. 214 (2000) 55–60.
[46] M.J. Iqbal, M.R. Siddiquah, J. Alloys Compd. 453 (2008) 513–518.
[47] D. Ravinder, K.S. Reddy, P. Mahesh, T.B. Rao, Y.C. Venudhar, J. Alloys Compd. 370 (2004) L17–L22.